Absolute *K*-shell ionization cross sections and $L\alpha$ and $L\beta_1$ x-ray production cross sections of Ga and As by 1.5–39-keV electrons

C. Merlet
ISTEEM, FR 2035, CNRS, Université de Montpellier II, Sciences et Techniques du Languedoc, Pl. E. Bataillon, 34095 Montpellier Cedex 5, France

X. Llovet*
Serveis Cientificotècnics, Universitat de Barcelona, Lluís Solé i Sabarís 1-3, 08028 Barcelona, Spain

J. M. Fernández-Varea
Facultat de Física (ECM), Universitat de Barcelona, Diagonal 647, 08028 Barcelona, Spain
(Received 6 April 2006; published 28 June 2006)

Absolute *K*-shell ionization and $L\alpha$ and $L\beta_1$ x-ray production cross sections for Ga and As have been measured for incident electrons in the energy range from 1.5 to 39 keV. The cross sections were deduced from $K\alpha$, $L\alpha$, and $L\beta_1$ x-ray intensities emitted from ultrathin GaAs samples deposited onto self-supporting carbon films. The x-ray intensities were measured on an electron microprobe equipped with several wavelength-dispersive spectrometers and were converted into absolute cross sections by using estimated values of the target thickness, spectrometer efficiency, and number of incident electrons. Experimental results are compared with cross sections calculated from the plane-wave and distorted-wave Born approximations, the relativistic binary-encounter-Bethe model, the results of two widely used simple analytical formulas, and, whenever possible, experimental data from the literature.

DOI: 10.1103/PhysRevA.73.062719 PACS number(s): 34.80.Dp

I. INTRODUCTION

Cross sections for the ionization of atomic inner shells by electron impact are needed for a number of applications, such as elemental analysis by electron probe microanalysis (EPMA) and Auger electron spectroscopy, for the characterization of x-ray sources employed in medical and industrial applications and, in general, for the simulation of radiation transport in matter.

Measurements of inner-shell ionization cross sections by electron impact have been reported in the literature for many years [1–3]; among other methods, the cross sections have been deduced from the x-ray intensity emitted in the deexcitation of atoms in thin-film targets. As a result, there is a large body of experimental information, especially near the ionization threshold. However, closer inspection of the experimental data reveals that a lot of it is on *K* shells [4]; measurements for *L* shells are comparatively very scarce, while there are almost no values for *M* shells. Indeed, whereas the *K* x-ray intensity is a function of only the cross section for *K*-shell ionization, *L*- and *M*-shell intensities depend simultaneously on the cross sections of the various subshells and therefore their extraction is more difficult. This dependence comes from the fact that vacancies in such shells can be produced not only by electron impact but also by Coster-Kronig (CK) transitions (nonradiative transitions between the corresponding subshells). Moreover, many *L* and *M* x-ray lines cannot be sufficiently resolved using solid-state x-ray detectors, in particular those emitted by low- and medium-*Z* elements. Accurate cross-section measurements for such shells and elements requires the use of high-resolution x-ray spectrometers such as the wavelength-dispersive (WD) spectrometer, but this has been used very rarely mainly because of the difficulties in determining its efficiency (with few exceptions [5]). The body of available inner-shell ionization data is not only scarce, but it is also affected by considerable uncertainties; results obtained by different groups often differ substantially more than the quoted uncertainties. These discrepancies make it difficult to check the reliability of calculation methods and predictive formulas, and call for a critical reexamination of existing experimental data [6]. New and more accurate experiments are therefore needed.

In the present study, we report experimental measurements of *K*-shell ionization and $L\alpha_{1,2}$ (hereafter referred to as $L\alpha$) and $L\beta_1$ x-ray production cross sections for Ga ($Z=31$) and As ($Z=33$) by impact of electrons with energies from 1.5 to 39 keV. The elements Ga and As were selected mainly because (i) no experimental results were found for the *K* shell of As and the *L* shells of Ga and As, and (ii) for the *K* shell of Ga, the only published set of experimental data [7] was found to fall about 50% below the predictions of the distorted-wave Born approximation (DWBA) [8]. [The DWBA is superior to the plane-wave Born approximation (PWBA) and other theoretical approaches based on the PWBA, and it has been shown to be in excellent agreement with a number of recent measurements [8–10].] The cross sections were obtained by recording $K\alpha$, $L\alpha$, and $L\beta_1$ x-ray intensities emitted from ultrathin GaAs samples deposited onto self-supporting C films, using an electron microprobe.

*Author to whom correspondence should be addressed. Electronic address: xavier@giga.sct.ub.es

In contrast to earlier studies by our group, in which the absolute value of the cross sections was obtained with a Si(Li) detector (see, e.g., Ref. [10]), here cross sections were extracted from measurements done only with WD spectrometers. The present cross sections are therefore expected to be more accurate than those obtained from earlier experiments, owing to the better spectral resolution of the WD spectrometer as compared to that of the Si(Li) detector. The efficiency of the WD spectrometers was estimated by comparing measurements and Monte Carlo simulations of thick-target bremsstrahlung spectra emitted from known targets [11], and the thickness of the irradiated films was determined by means of variable-voltage EPMA (see, e.g., Ref. [12]). Conversion of x-ray intensities to absolute cross sections was performed by using estimated values of the spectrometer efficiency, number of incident electrons, and target thickness. For the K shells, the ionization cross sections were extracted by using published fluorescence yields and x-ray emission rates. For the L shells, results are reported as cross sections for the production of the most intense lines: namely, the $L\alpha$ and $L\beta_1$ lines. Measured cross sections are compared with theoretical cross sections calculated from the DWBA, the PWBA, and the relativistic binary-encounter-Bethe (RBEB) model, with two analytical formulas widely used in many applications and, whenever possible, with existing experimental values. For comparison purposes, theoretical L-subshell ionization cross sections have been converted into $L\alpha$ and $L\beta_1$ x-ray production cross sections by using fluorescence yields, x-ray emission rates, and CK yields available in the literature.

II. EXPERIMENT

A. Experimental method

The methodology adopted for the present measurements is similar to that described in Ref. [10]. Briefly, we assume that electrons penetrate a self-supporting film of the studied element following a straight trajectory without losing energy. This assumption is plausible for very thin films and/or for electron beams with relatively large energies. The cross section for K-shell ionization, σ_K, is given by [13]

$$\sigma_K(E) = \frac{1}{\omega_K}\frac{\Gamma_{K\ \mathrm{total}}}{\Gamma_{KL_{2,3}}}\frac{4\pi}{\mathcal{N}tN_e\epsilon\Delta\Omega}N_{K\alpha}(E), \tag{1}$$

where ω_K is the fluorescence yield, $\Gamma_{KL_{2,3}}$ and $\Gamma_{K\ \mathrm{total}}$ are the x-ray emission rates for the transition $KL_{2,3}$ (which originates the $K\alpha$ line) and for all possible transitions to the K shell, respectively, $\mathcal{N}$ is the density of atoms in the target (atoms per unit volume), t is the film thickness, N_e and E are the number and energy of incident electrons, ϵ is the spectrometer efficiency, $\Delta\Omega$ is the solid angle of collection, and $N_{K\alpha}$ is the intensity of the $K\alpha$ line. The $L\alpha$ and $L\beta_1$ x-ray production cross sections $\sigma_{L\alpha}$ and $\sigma_{L\beta_1}$ are given by

$$\sigma_{L\alpha}(E) = \frac{4\pi}{\mathcal{N}tN_e\epsilon\Delta\Omega}N_{L\alpha}(E) \tag{2}$$

and

$$\sigma_{L\beta_1}(E) = \frac{4\pi}{\mathcal{N}tN_e\epsilon\Delta\Omega}N_{L\beta_1}(E), \tag{3}$$

where $N_{L\alpha}$ and $N_{L\beta_1}$ are the intensities of the $L\alpha$ and $L\beta_1$ lines, respectively.

B. Targets

Measured targets consisted of ultrathin GaAs films deposited on self-supporting C backing foils. The targets were obtained by vacuum evaporation of GaAs onto previously prepared self-supporting C backing films. The latter were, in turn, obtained by evaporating C onto mica sheets, extracting the C layers in distilled water, and, while they were floating on the water, placing them onto a grid of the kind used in transmission electron microscopy. The thickness of the C backing films (~20 nm) was reduced down to ~5 nm by ion milling, in attempts to minimize the contribution of backscattered electrons, especially at low incident electron energies (from 1.5 to 8 keV). Ion milling was done using a CAMECA IMS5F ion microprobe, and the area milled was $\sim 80 \times 80\ \mu\mathrm{m}^2$. During the GaAs evaporation runs, high-purity, polished Ni was also used as substrates; the resulting twin GaAs/Ni samples were employed to determine the thickness and composition of the target films by variable-voltage EPMA [12]. The reason for using the GaAs/Ni samples instead of GaAs/C(5 nm) films for thickness and composition determination is that the accuracy of variable-voltage EPMA largely improves when the atomic numbers of the film and substrate are similar. In this sense, every precaution was taken so as to estimate the target thickness as accurately as possible, as this is crucial for accurate cross-section measurements. Variable-voltage EPMA consists of measuring the x-ray intensity emitted by the film and substrate atoms at different electron incident energies. Experimental intensities are normalized to those emitted by reference samples containing the elements of interest and compared with the predictions of an x-ray emission model. The composition and film thickness are left as free parameters in the model, and by means of an iterative procedure, values of these parameters that yield x-ray intensities that best match the measurements are obtained.

In order to determine the thickness and composition of the GaAs/C(5 nm) targets, the intensities of the Ga, As, and Ni $L\alpha$ lines and Ga, As, and Ni $K\alpha$ lines emitted from the twin GaAs/Ni targets were recorded for electron incident energies from 1.5 to 39 keV and analyzed with the help of the analytical x-ray emission model described in Ref. [14]. The thicknesses of the GaAs films were found to be in the range 1–6 nm, with compositions of ~60 at. % Ga and ~40 at. % As. Such small thicknesses are required so as to minimize multiple scattering in the active film, which would lead to an increase of the x-ray intensity, especially at low incident energies [10]. Figure 1 shows the variation of the intensity ratio of the above-mentioned x-ray lines for a $Ga_{0.62}As_{0.38}$(5.6 nm)/Ni sample. The smoothness of measured x-ray intensity ratios as well as the good agreement

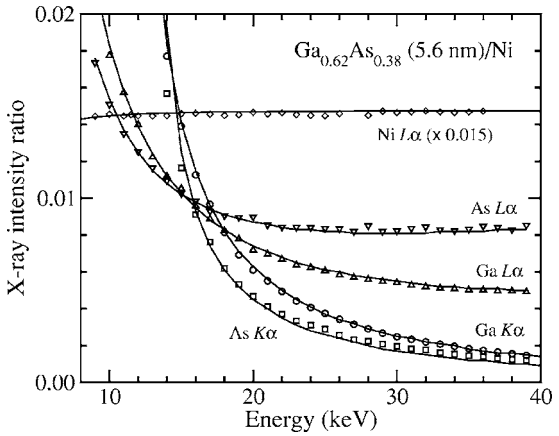

FIG. 1. X-ray intensity ratios for the Ga $L\alpha$, As $L\alpha$, Ga $K\alpha$, As $K\alpha$, and Ni $L\alpha$ lines emitted from a $Ga_{0.62}As_{0.38}$(5.6 nm)/Ni sample, as functions of the incident electron energy. The intensity ratios were determined with respect to pure GaAs and Ni reference samples. Symbols represent experimental data. Curves are results from Merlet's x-ray emission model [14], which yielded the thickness and composition of this particular target.

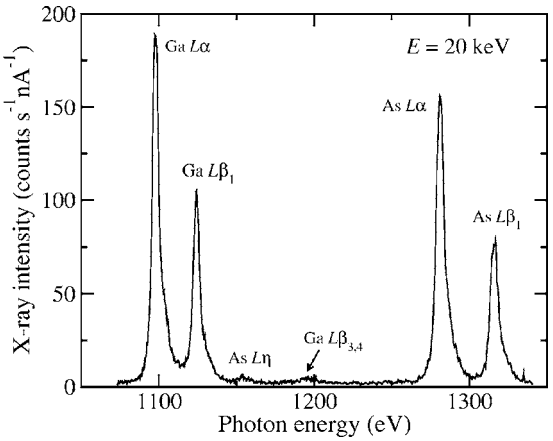

FIG. 2. Typical x-ray spectrum emitted from a $Ga_{0.62}As_{0.38}$(5.6 nm)/C(5 nm) sample, recorded with a TAP crystal.

with the predictions of the x-ray model over almost all the electron incident energies for the obtained values of film thickness and composition is noteworthy; as a result, the accuracy of the thickness and composition determination is estimated to be better than 5%.

Finally, to reduce a possible contribution of stray radiation coming from the interaction of transmitted electrons and x rays with the specimen chamber, a homemade Faraday cup was inserted below the sample so as to absorb transmitted electrons and x rays. The Faraday cup consisted of an 8-mm-diam C cylinder with 0.5-mm-thick, 2-cm-long Be lids, in which the upper lid had a 2.5-mm-diam hole.

C. X-ray measurements

All measurements were performed on a CAMECA SX-100 electron microprobe, equipped with five WD spectrometers, at the University of Montpellier II. In this instrument, the spectrometers are oriented so as to collect x rays that emerge in directions forming an angle of 40° with the sample surface; each spectrometer contains up to four different dispersing crystals. After being diffracted by the crystals, the x rays are detected with an Ar-CH_4 flow proportional counter and finally recorded with a pulse-height analyzer.

A typical L x-ray spectrum emitted from a $Ga_{0.62}As_{0.38}$(5.6 nm)/C(5 nm) target resulting from 20-keV electron bombardment is displayed in Fig. 2. The spectrum was recorded with a thallium acid phthalate (TAP) crystal. The observed x-ray lines originate from the filling of vacancies in the L shells due to transitions from M shells. For both elements Ga and As, the most intense lines are the $L\alpha$ and $L\beta_1$ lines, which correspond to the transitions $L_3M_{4,5}$ and L_2M_4, respectively. Two weaker lines—namely, As $L\eta$ and Ga $L\beta_{3,4}$, pertaining to the transitions L_2M_1 and $L_1M_{2,3}$, respectively—are also visible. The less visible, high-energy tails of the $L\alpha$ and $L\beta_1$ lines correspond to satellite lines, which arise from the decay of double-vacancy states. The As $L\ell$ line, which originates from the transition L_3M_1 (at 1119.5 eV), is not observed. Spectra were fitted with a combination of pseudo-Voigt functions (see, e.g., Ref. [15]) so as to describe both the diagram and satellites lines. This allowed us to optimize the x-ray intensity measurements as follows. Taking advantage of the fact that each WD line can be described by a pseudo-Voigt function, measurements were only performed at wavelength channels corresponding to the peak maxima, and peak areas N were estimated as

$$N = kI_G + (1-k)I_L, \tag{4}$$

with $0.4 < k < 0.9$ depending on the dispersing crystal and x-ray line, $I_G \approx N_{max} \times \Gamma \times 1.064$ and $I_L \approx N_{max} \times \Gamma \times 1.510$, where Γ is the full width at half maximum of the Gaussian and Lorentzian distributions, and N_{max} is the net counting rate at the peak maximum. The latter rate was obtained by subtracting the spectral background by linear interpolation of two measurements done close to the peak (on either side of it).

X-ray intensities were recorded from 1.5 keV to 39 keV in, at the most, 1-keV steps. Electron currents were 100 nA. For each accelerating voltage, measurements were carried out at ten positions, at least, on five different self-supporting films, with counting times typically of 600 s. The number of incident electrons was estimated by multiplying the reading of the electron current by the acquisition time. To avoid contamination during the experiments, a liquid-nitrogen cold finger was employed. The dispersing crystals used were a large lithium fluoride (LLiF) crystal for the measurement of Ga, As, and Ni $K\alpha$ x rays and a TAP crystal for Ga, As, and Ni $L\alpha$ and Ga and As $L\beta_1$ x rays. The values of the parameter k obtained from the fitting procedure [see Eq. (4)] were 0.8 for the LLiF crystal and 0.5 for the TAP crystal.

D. Spectrometer efficiency

The efficiency of the WD spectrometer was estimated as follows (for more details see Ref. [11]). Let $N(E)\mathrm{d}E$ denote

the number of bremsstrahlung photons with energies between E and $E+dE$, per incident electron, emitted by a thick, reference sample. The product of the spectrometer efficiency times the solid angle of collection, evaluated at the wavelength channel corresponding to $\lambda_i = hc/E_i$, can be obtained from the relation

$$\epsilon(\lambda_i)\Delta\Omega = \frac{N_i \Delta\lambda}{\int_{E(\lambda_i+\Delta\lambda)}^{E(\lambda_i)} N(E)dE}, \quad (5)$$

where $\Delta\lambda$ is the width of the wavelength channel and N_i is the number of photons detected at the channel $(\lambda_i, \lambda_i+\Delta\lambda)$ per incident electron.

In order to obtain the efficiency of the WD spectrometers from Eq. (5), bremsstrahlung intensities (N_i) were measured at wavelength channels corresponding to the peaks of interest ($K\alpha$, $L\alpha$, and $L\beta_1$ lines of Ga and As) on reference samples of C, Si, and Ni, at selected electron incident energies. The corresponding theoretical bremsstrahlung intensities $N(E)$ were then calculated using the general-purpose Monte Carlo simulation code PENELOPE [16], which implements bremsstrahlung cross sections based on relativistic, partial-wave calculations [17]. The particular reference samples were chosen because neither absorption edges nor spectral lines could be observed in a wide wavelength interval around the wavelengths of interest. By doing this, possible uncertainties in PENELOPE's mass attenuation coefficients near the absorption edges are minimized. For each beam energy and sample, measurements were performed at ten different sample positions, with counting times long enough to ensure that the statistical uncertainties were less than 1%. A correction was applied [11] to minimize the effects of stray radiation, higher-order Bragg reflections [18] and total reflection [19].

E. Uncertainties of cross-section measurements

Experimental cross sections are affected by random uncertainties arising from counting statistics, sample nonuniformity, stray radiation, and instrumental drift. From repeated measurements, random uncertainties were estimated to be ~1% (Ga K line), ~3% (As K line), ~1.5% (Ga L lines), and ~4% (As L lines), except very close to the ionization threshold, where uncertainties are larger due to the low x-ray intensities. Conversion of x-ray intensities to absolute cross sections introduces uncertainties of a systematic nature. These are essentially the same for all incident electron energies, and therefore they originate a shift of the cross-section curves (without affecting their shape). Systematic uncertainties come from the adopted values for the target thickness and composition (5%), number of incident electrons (2%), and detector efficiency (10%). The latter uncertainty mainly arises from that of the bremsstrahlung cross sections implemented in PENELOPE, which are essentially based on the tabulation of Kissel *et al.* [17] (and are believed to have an uncertainty of 10%). Nevertheless, the uncertainty in the spectrometer efficiency estimation for the K lines of Ga and As is probably less than the quoted value, since bremsstrahlung spectra measured with a Si(Li) detector around such lines, emitted from the reference targets considered (C, Si, and Ni), have been found to agree with those calculated using PENELOPE to within less than 5% [20,21]. For the K shells, added to these uncertainties are those coming from the adopted fluorescence yields (3%) and x-ray emission rates (2%), which were taken from Refs. [22,23], respectively (see Table I). The global uncertainties, obtained by combining random and systematic contributions in quadrature, were ~12% for both the K and L shells.

TABLE I. K fluorescence yields and x-ray emission rates for Ga and As adopted in this study.

	ω_K	$\Gamma_{KL_{2,3}}/\Gamma_{K\ \mathrm{total}}$
Ga	0.496	0.872
As	0.549	0.865

III. THEORETICAL CALCULATIONS

For the sake of completeness, in the present work we have also evaluated the ionization cross sections for the studied shells of Ga and As by means of various theoretical procedures. Some of them are *ab initio* models that involve numerical calculations, whereas the others are analytical formulas based either on simple models or on fits to experimental data.

The first theoretical approach considered is the DWBA, as implemented by Segui *et al.* [8]. In the DWBA, the interaction between the projectile and the active atomic electron is treated using first-order perturbation theory with wave functions for the initial and final states of the projectile that include the distortion caused by the potential of the target atom. In addition, the DWBA allows a consistent description of exchange effects. As a consequence of these features, the approximation is expected to yield accurate results even close to the ionization threshold. However, the corresponding numerical calculations are time consuming and, at present, convergence problems limit the applicability of the method to kinetic energies below about 10 times the ionization energy of the considered shell. An important reduction in the numerical burden of the DWBA is achieved by the PWBA, in which the initial and final states of the projectile are represented by plane waves instead of distorted waves. The ensuing PWBA calculations are therefore doable up to much larger incident kinetic energies than for the DWBA counterpart. Ionization cross sections evaluated with the PWBA are reliable for high-energy electrons, but due to the simplifying assumptions and the neglect of exchange effects, they become less accurate near the threshold energy.

The present DWBA and PWBA calculations have been carried out using Dirac-Hartree-Slater (DHS) self-consistent atomic potentials; correlation effects are relatively unimportant for inner shells, and thus DHS potentials are realistic enough for our purposes. The radial Dirac equation has been

solved numerically, with the aid of the RADIAL subroutine package [24], for the initial (bound) and final (free) wave functions of the active electron and, in the case of the DWBA, also for the (free) wave functions of the projectile electron. A sufficient number of terms in the partial-wave expansions were summed up so as to attain an accuracy better than 1% and 0.1% in the DWBA and PWBA cross sections, respectively. Further details of the numerical evaluation of ionization cross sections within these formalisms can be found in Refs. [8,25], respectively.

The numerical PWBA calculations discussed above are still too cumbersome for practical applications. Consequently, much effort has been devoted over the years to devise analytical or semianalytical expressions to evaluate ionization cross sections by resorting to simplified versions of the PWBA. For instance, Hippler [26] proposed the use of the (nonrelativistic) hydrogenic generalized oscillator strength to describe *K*-shell electrons, together with simple exchange and Coulomb corrections that improve the behavior of the model near the ionization threshold. The resulting semianalytical approach compares rather well with existing experimental information on *K*-shell cross sections [27]. We have implemented the model outlined by Hippler [26] including relativistic effects in the kinematics of the projectile electron [27]. It is worth mentioning that, although this model has been extended to deal with the ionization of *L* and *M* subshells (see, e.g., Ref. [28]), it is expected to be less reliable in these cases due to the worsening of the hydrogenic approximation (as the screening of the nuclear attraction by the deeper atomic shells increases).

Another theoretical approach that has been receiving considerable attention recently is the RBEB model of Kim and co-workers [29], which is also based on the PWBA supplemented with several judicious simplifications that yield an analytical expression for the ionization cross section. The RBEB model provides fairly realistic cross sections for the ionization of *K* shells by electron impact [30]. The average kinetic energies of the electrons in the *K* shell and *L* subshells required to evaluate the respective RBEB cross sections were taken from Ref. [30] and from the aforementioned DHS self-consistent calculations, respectively.

As a widely used representative of an analytical formula based on empirical fits to experimental ionization cross sections we have chosen the expression given by Casnati *et al.* [31]. It should be mentioned that this formula was derived to predict *K*-shell ionization, but it has been commonly employed and even recommended for *L* and other outer shells [32]. For this reason we have used it here for both *K* and *L* shells. Finally, among the wealth of simpler approaches that yield an analytical expression for the ionization cross section, the semiclassical model by Gryzinski [33] is still extensively used in many applications and it has also been included in our study.

IV. RESULTS AND DISCUSSION

In this section, we compare our measurements (collected in Table II) with the above-mentioned theoretical calculations and analytical formulas, and with experimental results by other authors.

A. *K*-shell ionization

Figure 3(a) compares our experimental *K*-shell ionization cross section for Ga with the predictions of the DWBA, the RBEB and Hippler's models, the formulas of Casnati *et al.* and Gryzinski, and the measurements of Zhou *et al.* [7]. The experimental data are plotted with representative absolute uncertainties. We can see that the DWBA calculations are in excellent agreement with the present measurements, in both relative and absolute terms. The RBEB model lies ~10% below our experimental values whereas Hippler's cross section is ~10% higher than our measured data. In turn, the formulas of Casnati *et al.* and Gryzinski are ~10% higher and ~20% lower, respectively, than our measurements. It is also observed that the experimental cross sections of Zhou *et al.* [7] are about 50% lower than our results; this discrepancy greatly exceeds the uncertainties quoted by these authors. Comparison of the present experimental *K*-shell ionization cross section for As with the aforesaid calculations is shown in Fig. 3(b). Here, no experimental data from other authors were found to compare them with. It is seen that the predictions of the DWBA are in fair agreement, within the uncertainty bars, with the present measurements both in absolute and relative terms. The good agreement as regards the shape of the DWBA cross-section curve can be assessed by rescaling the experimental data by a factor of 1.04. The RBEB and Hippler's simplified forms of the PWBA, the formula of Gryzinski, and that of Casnati *et al.* follow the same trends as those found for Ga. It should be pointed out that, with the exception of the DWBA, none of the calculated cross sections considered is capable of satisfactorily reproducing the shape of the experimental Ga and As cross-section curves.

B. *L*-shell x-ray production

As already mentioned, vacancy states in the *L* shells can be produced not only by direct electron impact, but also by CK transitions and, to a lesser extent, by radiative and nonradiative transitions to the *K* shell and by radiative transitions between L_i subshells. The cross sections for production of $L\alpha$ and $L\beta_1$ x rays, $\sigma_{L\alpha}$ and $\sigma_{L\beta_1}$, respectively, are given by

$$\sigma_{L\alpha} = \frac{\Gamma_{L_3M_{4,5}}}{\Gamma_{L_3\ \mathrm{total}}}\omega_{L_3}[n_{KL_3}\sigma_K + (f_{13} + f_{12}f_{23} + f'_{13})\sigma_{L_1} + f_{23}\sigma_{L_2} + \sigma_{L_3}] \tag{6}$$

and

$$\sigma_{L\beta_1} = \frac{\Gamma_{L_2M_4}}{\Gamma_{L_2\ \mathrm{total}}}\omega_{L_2}[n_{KL_2}\sigma_K + f_{12}\sigma_{L_1} + \sigma_{L_2}], \tag{7}$$

where $\Gamma_{L_3M_{4,5}}$ and $\Gamma_{L_3\ \mathrm{total}}$ are the x-ray emission rates for the transition $L_3M_{4,5}$ and for all possible transitions to the L_3 subshell, respectively, $\Gamma_{L_2M_4}$ and $\Gamma_{L_2\ \mathrm{total}}$ are the correspond-

TABLE II. Measured K-shell ionization cross sections and $L\alpha$ and $L\beta_1$ x-ray production cross sections for Ga and As by electron impact.

E (keV)	Ga σ_K (barn)	As σ_K (barn)	Ga $\sigma_{L\alpha}$ (barn)	As $\sigma_{L\alpha}$ (barn)	Ga $\sigma_{L\beta_1}$ (barn)	As $\sigma_{L\beta_1}$ (barn)
1.5			290	83	167	49
2.0			547	332	271	219
2.5			627	431	327	
3.0			675	559	344	314
4.0			669	656	347	343
5.0			646	652	331	330
6.0			610	642	316	326
7.0			573	608	295	311
8.0			539	582	279	290
9.0			517	559	263	276
10.0			485	530	250	262
10.5	10		474	510		
11.0	39		469	503	242	246
11.5	70		449	484		
12.0	92	4	442	482	225	241
13.0	134	49	421	468	215	227
14.0	166	83	403	450	202	218
15.0	193	109	387	426	191	213
16.0	214	131	371	413	187	200
17.0	234	151	358	394	180	190
18.0	251	168	346	382	173	188
19.0	260	181	334	374	167	181
20.0	276	194	321	368	160	176
21.0	281	201	312	350	155	167
22.0	289	209	302	339	154	167
23.0	296	216	291	331	148	162
24.0	302	226	284	327	144	152
25.0	310	235	277	316	142	152
26.0	309	233	271	305	139	150
27.0	316	231	263	296	134	142
28.0	316	242	257	295	131	140
29.0	320	248	254	283	128	142
30.0	320	249	249	276	125	134
31.0	322	250	243	273	123	132
32.0	324	258	239	270	121	128
33.0	324	253	230	259	118	129
34.0	325	253	226	252	116	126
35.0	324	253	224	248	113	120
36.0	325	258	220	246	111	112
37.0	328	254	216	233	109	119
38.0	328	256	212	229	108	115
39.0	323	258	208	231	106	108

ing rates for the transition L_2M_4 and for all possible transitions to the L_2 subshell, ω_{L_3} and ω_{L_2} are the fluorescence yields for the L_3 and L_2 subshells, n_{KL_3} and n_{KL_2} are the radiative plus nonradiative yields for transitions of vacancies from the K shell to the L_3 and L_2 subshells, f_{12}, f_{13}, and f_{23} are the CK yields between the L_1, L_2, and L_3 subshells, and f'_{13} is the intrashell radiative yield for transitions of vacancies from the L_1 subshell to the L_3 subshell [the contribution of

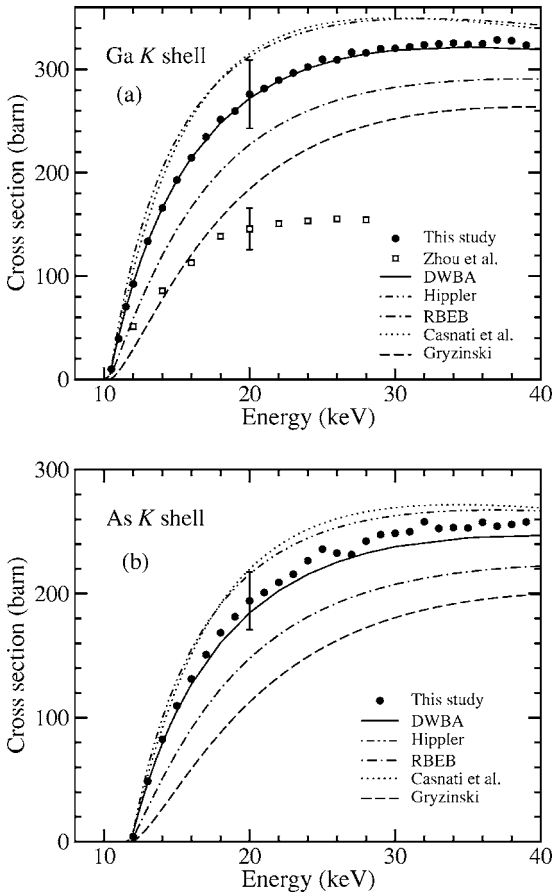

FIG. 3. Absolute *K*-shell ionization cross section vs incident electron energy for Ga (a) and As (b). Solid circles are the present experimental values. Solid and double-dot-dashed curves are the predictions of the present DWBA calculations and Hippler's model, respectively; dot-dashed curves correspond to the RBEB model; dotted and dashed curves are the results from the formulas of Casnati *et al.* and Gryzinski, respectively. Open squares are measurements by Zhou *et al.* [7].

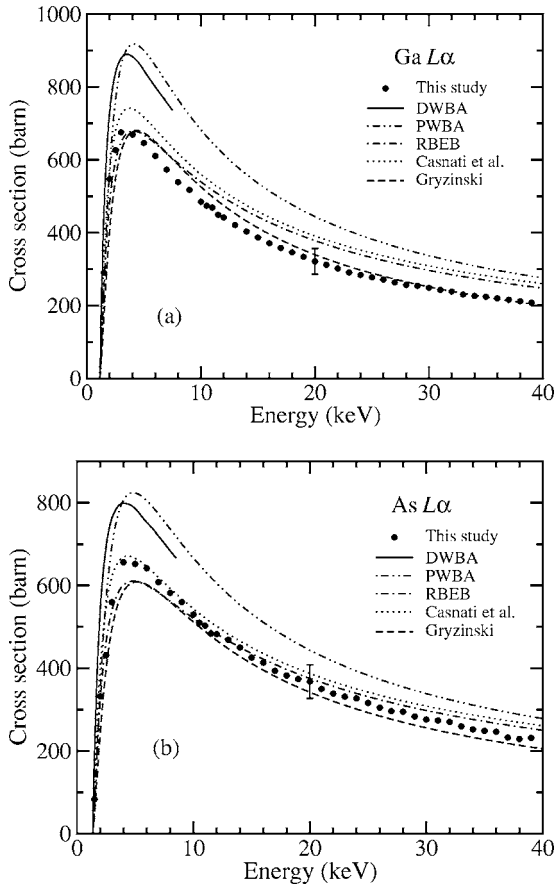

FIG. 4. Absolute $L\alpha$ x-ray production cross sections vs incident electron energy for Ga (a) and As (b). Solid circles are the present measurements. Solid and double-dot-dashed curves are the present DWBA and PWBA calculations, respectively; dot-dashed curves correspond to the RBEB model; dotted and dashed curves indicate the results from the formulas of Casnati *et al.* and Gryzinski, respectively.

other intrashell radiative transitions has been excluded in Eqs. (6) and (7) because of the extremely low values of the corresponding yields].

In order to facilitate comparison with the experimental measurements, theoretical *L*-subshell ionization cross sections obtained from the approaches discussed in the previous section have been converted into $L\alpha$ and $L\beta_1$ x-ray production cross sections through Eqs. (6) and (7). To this end, we have adopted atomic relaxation parameters from the latest compilations available in the literature. Namely, the *L* x-ray emission rates have been taken from Ref. [34] (which are values interpolated from calculations performed by Scofield [35]), the radiative and nonradiative yields for vacancies of the *K* shell to the L_2 and L_3 subshells from Ref. [36], and the intrashell radiative yields from Ref. [37]. It should be mentioned that the recent tabulation by Campbell [38] does not provide any new recommended values of the fluorescence yields and CK coefficients for Ga and As. Hence, we have adopted the earlier (semiempirical) compilation by Krause [37] instead of the DHS calculations of Chen *et al.* [39], which are also available. The relaxation parameters employed in this study are shown in Table III.

When comparing x-ray production cross sections with the experimental data, the fact that the adopted relaxation parameters are affected by sizable uncertainties should be kept in mind. Estimates of such uncertainties are given by Krause in

TABLE III. *L* fluorescence yields, radiative, and nonradiative yields for transitions of vacancies from the *K* shell to the *L* subshells, CK yields, intrashell radiative yields, and x-ray emission rates adopted in this work.

	ω_{L_2}	ω_{L_3}	n_{KL_2}	n_{KL_3}	f_{12}	f_{13}	f_{23}	f'_{13}	$\Gamma_{L_2M_4}/\Gamma_{L_2\ \text{total}}$	$\Gamma_{L_3M_{4,5}}/\Gamma_{L_3\ \text{total}}$
Ga	0.012	0.013	0.476	0.647	0.29	0.53	0.032	3.0E−5	0.953	0.957
As	0.014	0.016	0.442	0.639	0.28	0.53	0.063	3.4E−5	0.950	0.953

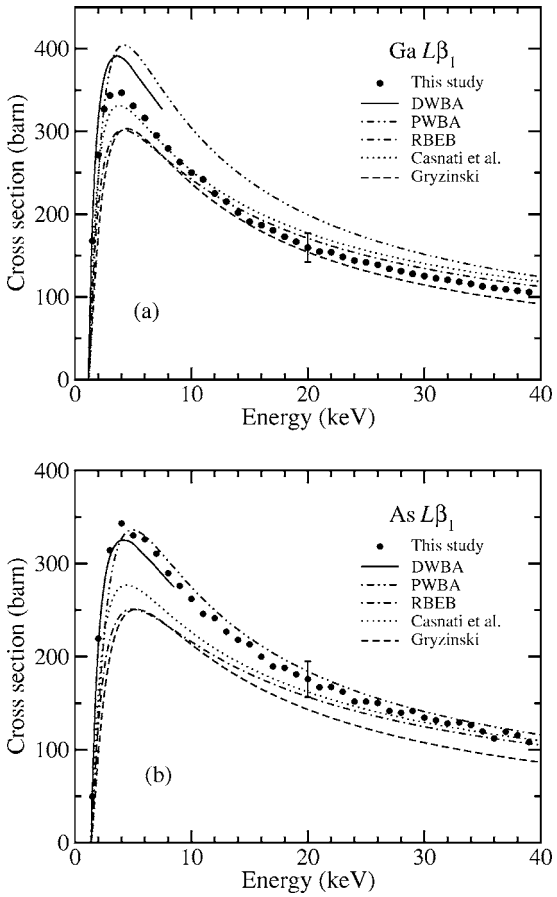

FIG. 5. Absolute $L\beta_1$ x-ray production cross sections vs incident electron energy for Ga (a) and As (b). Solid circles are the present measurements. Solid and double-dot-dashed curves are the present DWBA and PWBA calculations, respectively; dot-dashed curves correspond to the RBEB model; dotted and dashed curves indicate the results from the formulas of Casnati *et al.* and Gryzinski, respectively.

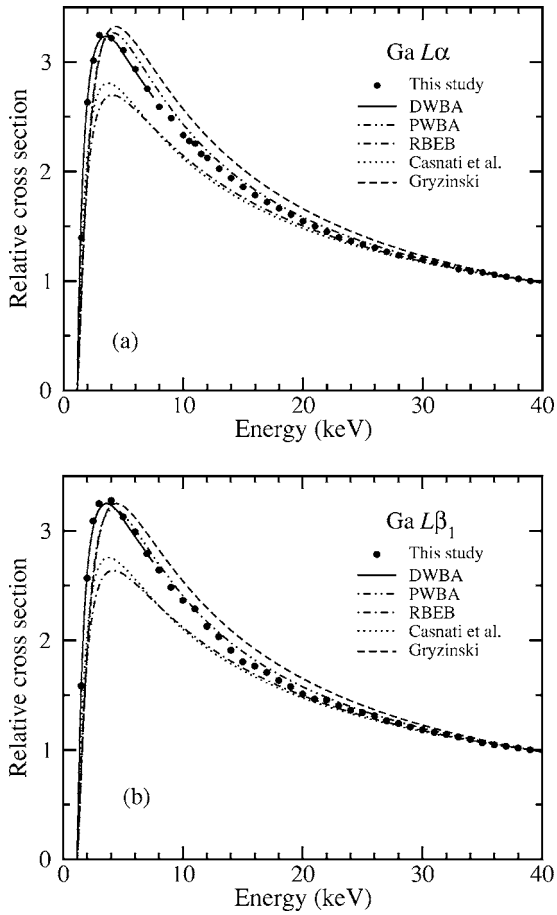

FIG. 6. Relative Ga $L\alpha$ (a) and Ga $L\beta_1$ (b) cross sections as a function of the incident electron energy (normalized as explained in the text). Solid circles are the present measurements. Solid and double-dot-dashed curves are the present DWBA and PWBA calculations, respectively; dot-dashed curves correspond to the RBEB model; dotted and dashed curves indicate the results from the formulas of Casnati *et al.* and Gryzinski, respectively.

Ref. [37] and, for Ga and As, are the following: 20% for ω_{L_3}, 25% for ω_{L_2}, 15% for f_{12}, 10% for f_{13}, and 20%–30% for f_{23}. Moreover, molecular effects can also affect fluorescence yields and CK coefficients for such elements [40]. Therefore, each calculated x-ray production cross section should actually be regarded as a "band" with a given uncertainty width. In fact, if we had extracted the subshell ionization cross sections from the experimental x-ray intensities, we would have had to add such uncertainties to those arising from the measurement itself.

Figures 4 and 5 display a comparison of the experimental $L\alpha$ and $L\beta_1$ x-ray production cross sections for Ga and As with the theoretical results of the DWBA and PWBA, the RBEB model, and the formulas of Casnati *et al.* and Gryzinski, computed by using the relaxation parameters shown in Table III. As before, the plotted uncertainty bars represent the global uncertainties of the present measurements. No experimental data were found in the literature to compare them with. We recall that the DWBA as implemented by Segui *et al.* [8] does not allow the calculation of cross sections for energies beyond ~10 times the ionization threshold. In particular, the DWBA cross sections calculated for the L shells of Ga and As stop at ~8 keV. (Here it should be mentioned that in an earlier study [10] we merged the results of the DWBA with those of the PWBA at higher energies; however, in the present study both calculations are shown separately.) From Figs. 4 and 5 it is seen that for Ga and As $L\alpha$ as well as for Ga $L\beta_1$, the formulas of Gryzinski and Casnati *et al.* and the RBEB model show good agreement with our experimental data, as regards the magnitude of the cross section. Conversely, the predictions of the DWBA and PWBA overestimate the present measurements by percentages in the range of 10%–20% and 12%–25%, respectively. These features are not observed for the As $L\beta_1$ cross section [Fig. 5(b)], for which the experimental values follow the trends of the PWBA and DWBA calculations, while the rest of the approximations underestimate the measured data. Nevertheless, it is apparent that for all the studied shells (including the K shells) our experimental data are systematically ~5% higher for As than for Ga, relative to any of the calculated cross sections, and this tendency is also consistently observed for the As $L\beta_1$ cross section. In spite of this, the uncertainties in the fluorescence yields and CK coefficients

adopted for calculating the *L* x-ray production cross sections make it difficult to draw a definite conclusion about the reliability of the different *L*-subshell ionization cross-section calculations.

Figure 6 shows a comparison of measured and calculated Ga $L\alpha$ and $L\beta_1$ cross sections, normalized to their corresponding values at 39 keV (except for the DWBA cross sections, which have been normalized to the respective experimental cross-section values at 7 keV). For both x-ray lines, it is seen that the shape of the measured cross sections is in fair agreement with the DWBA (near the ionization threshold) and the PWBA (at higher electron incident energies). This trend is consistent with that found in our earlier study for Ge $L\alpha$ [10] and has also been observed for As $L\alpha$ and $L\beta_1$ (not included here for the sake of brevity).

V. CONCLUSIONS

In conclusion, we have performed measurements of the *K*-shell ionization and the $L\alpha$ and $L\beta_1$ x-ray production cross sections for Ga and As, for electrons with kinetic energies from 1.5 keV up to 39 keV. The relative and absolute uncertainties of the experimental values have been quoted to be 1%–4% and ~12%, respectively. For the *K* shells of the studied elements, we have shown that the predictions of the DWBA as developed by Segui *et al.* [8] are in excellent agreement with our measurements, in both relative and absolute terms. For the *L* shells considered, the DWBA and PWBA reproduce the shape of the present experimental data well, but these *ab initio* approaches overestimate the magnitude of the measured values. In contrast, the formulas of Gryzinski and Casnati *et al.* as well as the RBEB model reproduce the magnitude of the reported measurements much better, but not the corresponding shape. Nevertheless, the large uncertainties in the adopted fluorescence yields and CK coefficients, required to calculate the x-ray production cross sections from the subshell ionization cross sections, make it difficult to draw a definite conclusion about the reliability of the calculations for the *L* shells.

ACKNOWLEDGMENTS

We would like to thank Francesc Salvat for allowing us to use his DWBA code and for critically reading the manuscript. This work has been partially supported by the Spanish Fondo de Investigación Sanitaria (Project No. 03/0676).

[1] C. J. Powell, Rev. Mod. Phys. **48**, 33 (1976).
[2] C. J. Powell, in *Electron Impact Ionization*, edited by T. D. Märk and D. H. Dunn (Springer-Verlag, Berlin, 1985), Chap. 6.
[3] C. J. Powell, in *Microbeam Analysis*, edited by J. R. Michael and P. Ingram (San Francisco Press, San Francisco, 1990).
[4] M. T. Liu, Z. An, C. H. Tang, Z. M. Luo, X. F. Peng, and X. G. Long, At. Data Nucl. Data Tables **76**, 213 (2000).
[5] S. Reusch, H. Genz, W. Löw, and A. Richter, Z. Phys. D: At., Mol. Clusters **3**, 379 (1986).
[6] C. J. Powell (private communication).
[7] G. G. Zhou, Z. An, and Z. M. Luo, J. Phys. B **35**, 841 (2002).
[8] S. Segui, M. Dingfelder, and F. Salvat, Phys. Rev. A **67**, 062710 (2003).
[9] C. S. Campos, M. A. Z. Vasconcellos, X. Llovet, and F. Salvat, Phys. Rev. A **66**, 012719 (2002).
[10] C. Merlet, X. Llovet, and F. Salvat, Phys. Rev. A **69**, 032708 (2004).
[11] C. Merlet and X. Llovet, Microchim. Acta (to be published).
[12] A. P. Mackenzie, Rep. Prog. Phys. **56**, 557 (1993).
[13] K. Shima, T. Nakagawa, K. Umetani, and T. Mikumo, Phys. Rev. A **24**, 72 (1981).
[14] cC. Merlet, in *Proceedings of the 29th Annual Conference of the Microbeam Analysis Society*, edited by E. S. Etz (VHC, New York, 1995) p. 203.
[15] C. Fournier, C. Merlet, O. Dugne, and M. Fialin, J. Anal. At. Spectrom. **14**, 381 (1999).
[16] F. Salvat, J. M. Fernández-Varea, and J. Sempau, PENELOPE, a code system for Monte Carlo simulation of electron and photon transport, OECD/NEA Data Bank, Issy-les-Moulineaux, France, 2003.
[17] L. Kissel, C. A. Quarles, and R. H. Pratt, At. Data Nucl. Data Tables **28**, 381 (1983).
[18] D. G. W. Smith and S. J. B. Reed, X-Ray Spectrom. **10**, 198 (1981).
[19] W. P. Rehbach and P. Karduck, in *Microbeam Analysis*, edited by J. R. Michael and P. Ingram (San Francisco Press, San Francisco, 1990), p. 135.
[20] E. Acosta, X. Llovet, E. Coleoni, J. A. Riveros, and F. Salvat, J. Appl. Phys. **83**, 6038 (1998).
[21] X. Llovet, L. Sorbier, C. S. Campos, E. Acosta, and F. Salvat, J. Appl. Phys. **93**, 3844 (2003).
[22] J. H. Hubbell, P. N. Trehan, N. Singh, B. Chand, D. Mehta, M. L. Garg, R. R. Garg, S. Singh, and S. Puri, J. Phys. Chem. Ref. Data **23**, 339 (1994).
[23] J. H. Scofield, Phys. Rev. A **9**, 1041 (1974).
[24] F. Salvat, J. M. Fernández-Varea, and W. Williamson, Jr., Comput. Phys. Commun. **90**, 151 (1995).
[25] S. Segui, M. Dingfelder, J. M. Fernández-Varea, and F. Salvat, J. Phys. B **35**, 33 (2002).
[26] R. Hippler, Phys. Lett. A **144**, 81 (1990).
[27] Z. An, Z. M. Luo, and C. Tang, Nucl. Instrum. Methods Phys. Res. B **179**, 334 (2001).
[28] S. P. Khare and J. M. Wadehra, Can. J. Phys. **74**, 376 (1996).
[29] Y.-K. Kim, J. P. Santos, and F. Parente, Phys. Rev. A **62**, 052710 (2000).
[30] J. P. Santos, F. Parente, and Y.-K. Kim, J. Phys. B **36**, 4211 (2003).
[31] E. Casnati, A. Tartari, and C. Baraldi, J. Phys. B **15**, 155 (1982).
[32] M. P. Seah and I. S. Gilmore, Surf. Interface Anal. **26**, 815 (1998).
[33] M. Gryzinski, Phys. Rev. **138**, A336 (1965).
[34] J. L. Campbell and J.-X. Xang, At. Data Nucl. Data Tables **43**,

281 (1989).
[35] J. H. Scofield, Phys. Rev. A **10**, 1507 (1974); **12**, 345(E) (1975).
[36] P. V. Rao, M. H. Chen, and B. Crasemann, Phys. Rev. A **5**, 997 (1972).
[37] M. O. Krause, J. Phys. Chem. Ref. Data **8**, 307 (1979).
[38] J. L. Campbell, At. Data Nucl. Data Tables **85**, 291 (2003).
[39] M. H. Chen, B. Crasemann, and H. Mark, Phys. Rev. A **24**, 177 (1981).
[40] C. A. Quarles and L. Estep, Phys. Rev. A **34**, 2488 (1986).